Immunoproteasome deficiency is a feature of non-small cell lung cancer with a mesenchymal phenotype and is associated with a poor outcome

Satyendra C. Tripathi[a], Haley L. Peters[b], Ayumu Taguchi[c], Hiroyuki Katayama[a], Hong Wang[a], Amin Momin[a], Mohit Kumar Jolly[d], Muge Celiktas[a], Jaime Rodriguez-Canales[c], Hui Liu[c], Carmen Behrens[c], Ignacio I. Wistuba[c], Eshel Ben-Jacob[d,1], Herbert Levine[d,2], Jeffrey J. Molldrem[b], Samir M. Hanash[a], and Edwin J. Ostrin[e,2]

[a]Department of Clinical Cancer Prevention, University of Texas M. D. Anderson Cancer Center, Houston, TX 77030; [b]Department of Stem Cell Transplantation and Cellular Therapy, University of Texas M. D. Anderson Cancer Center, Houston, TX 77030; [c]Department of Translational Molecular Pathology, University of Texas M. D. Anderson Cancer Center, Houston, TX 77030; [d]Center for Theoretical Biological Physics, Rice University, Houston, TX; and [e]Department of Pulmonary Medicine, University of Texas M. D. Anderson Cancer Center, Houston, TX 77030

Contributed by Herbert Levine, January 26, 2016 (sent for review November 5, 2015; reviewed by Eleftherios Diamandis, Beatrice S. Knudsen, and Jean Paul Thiery)

The immunoproteasome plays a key role in generation of HLA peptides for T cell-mediated immunity. Integrative genomic and proteomic analysis of non-small cell lung carcinoma (NSCLC) cell lines revealed significantly reduced expression of immunoproteasome components and their regulators associated with epithelial to mesenchymal transition. Low expression of immunoproteasome subunits in early stage NSCLC patients was associated with recurrence and metastasis. Depleted repertoire of HLA class I-bound peptides in mesenchymal cells deficient in immunoproteasome components was restored with either IFNγ or 5-aza-2′-deoxycytidine (5-aza-dC) treatment. Our findings point to a mechanism of immune evasion of cells with a mesenchymal phenotype and suggest a strategy to overcome immune evasion through induction of the immunoproteasome to increase the cellular repertoire of HLA class I-bound peptides.

immunoproteasome | NSCLC | EMT | immunotherapy

Proteasomes are multisubunit complexes that degrade intracellular proteins through the ubiquitin–proteasome pathway (1). The three catalytic β subunits β1, β2, and β5 in the proteasome complex are replaced by proteasome (prosome, macropain) subunit B9 (PSMB9)/β1i, PSMB10/β2i, and PSMB8/β5i, respectively, to form the immunoproteasome (2). The immunoproteasome generates peptides suitable for binding onto HLA I molecules, facilitating antigen presentation for $CD8^+$ T-cell responses. Lack of expression or down-regulation of the immunoproteasome may contribute to immune evasion through antigen loss (3).

The impact of immunoproteasome expression on antigen presentation in tumors of epithelial origin is not well established. We have investigated the constitutive and induced expression patterns of immunoproteasome subunits in non-small cell lung carcinoma (NSCLC) and their impact on antigen presentation. We provide evidence for dysregulated expression of immunoproteasome subunits in NSCLC cells with a mesenchymal phenotype, associated with a markedly reduced repertoire of HLA-bound peptides. Reduced expression of immunoproteasome subunits in NSCLC was also associated with reduced disease free survival.

Results

NSCLC Subgroups Can Be Defined Based on Their Immunoproteasome Gene Expression. Expression levels of 49 genes representing proteasome and immunoproteasome subunits across 42 NSCLC cell lines encompassing the heterogeneity of known driver mutations (*SI Appendix*, Section 1) were derived from global gene expression profiles (4, 5) [Gene Expression Omnibus (GEO) accession no. GSE32863] and subjected to unsupervised clustering analysis. Two prominent statistically significant clusters were observed on the basis of high and low expression of immunoproteasome specific subunits (Fig. 1 *A* and *B*). No significant differences were observed for proteasome subunits between these two groups. We also observed a significantly reduced expression of the immunoproteasome regulators *IRF1* and *STAT1* in the immunoproteasome low versus high cell lines (Fig. 1*C*). EGFR-mutated cell lines showed significantly higher expression of *PSMB8* and *PSMB9* compared with cell lines wild type for EGFR and KRAS mutations (Fig. 1*D*). No significant association was observed between KRAS mutation and expression of the immunoproteasome subunits. Ingenuity Pathway Analysis (IPA) (Qiagen; http://www.ingenuity.com) using differential gene expression revealed concordant down-regulation of several pathways, including antigen presentation and cell adhesion, with up-regulation of proliferation, metastasis, and mesenchymal lineage pathways (Dataset S1). Analysis of a dataset for EGFR inhibitor-sensitive and -resistant clones of the lung cancer cell line PC9 (GSE34228) revealed a significant reduction in immunoproteasome expression with the acquisition of EGFR-inhibitor resistance (*SI Appendix*, Fig. S1) (6).

Immunoproteasome-Low Cell Lines Exhibit a Mesenchymal Phenotype. In cell culture, immunoproteasome-low cell lines, as determined by gene

Significance

The success rate of therapeutic trials that target tumor antigens is quite limited. We demonstrate for the first time to our knowledge that lung cancer cells that have undergone epithelial-to-mesenchymal transition lose immunoproteasome expression, resulting in markedly reduced antigen presentation. Reduced expression of the immunoproteasome was associated with and can predict poor outcome in non-small cell lung carcinoma (NSCLC) patients. Induction of the immunoproteasome with IFNγ or 5-aza-2′-deoxycytidine (5-aza-dC) treatment can overcome this immune escape mechanism of mesenchymal cells by restoring functional HLA class I-bound peptides. These findings have substantial relevance for development of effective strategies to target tumor cells with inherent resistance to T cell-mediated immunotherapy.

Author contributions: S.C.T. and E.J.O. designed research; S.C.T., H.L.P., H.K., H.W., M.K.J., M.C., H. Liu, and E.J.O. performed research; S.C.T., H.L.P., A.M., J.R.-C., C.B., I.I.W., E.B.-J., H. Levine, J.J.M., and E.J.O. analyzed data; and S.C.T., A.T., S.M.H., and E.J.O. wrote the paper.

Reviewers: E.D., Mt. Sinai Hospital; B.S.K., Cedars-Sinai Medical Center; and J.P.T., National University of Singapore.

The authors declare no conflict of interest.

[1]Deceased June 5, 2015.

[2]To whom correspondence may be addressed. Email: herbert.levine@rice.edu or EJOstrin@mdanderson.org.

This article contains supporting information online at www.pnas.org/lookup/suppl/doi:10.1073/pnas.1521812113/-/DCSupplemental.

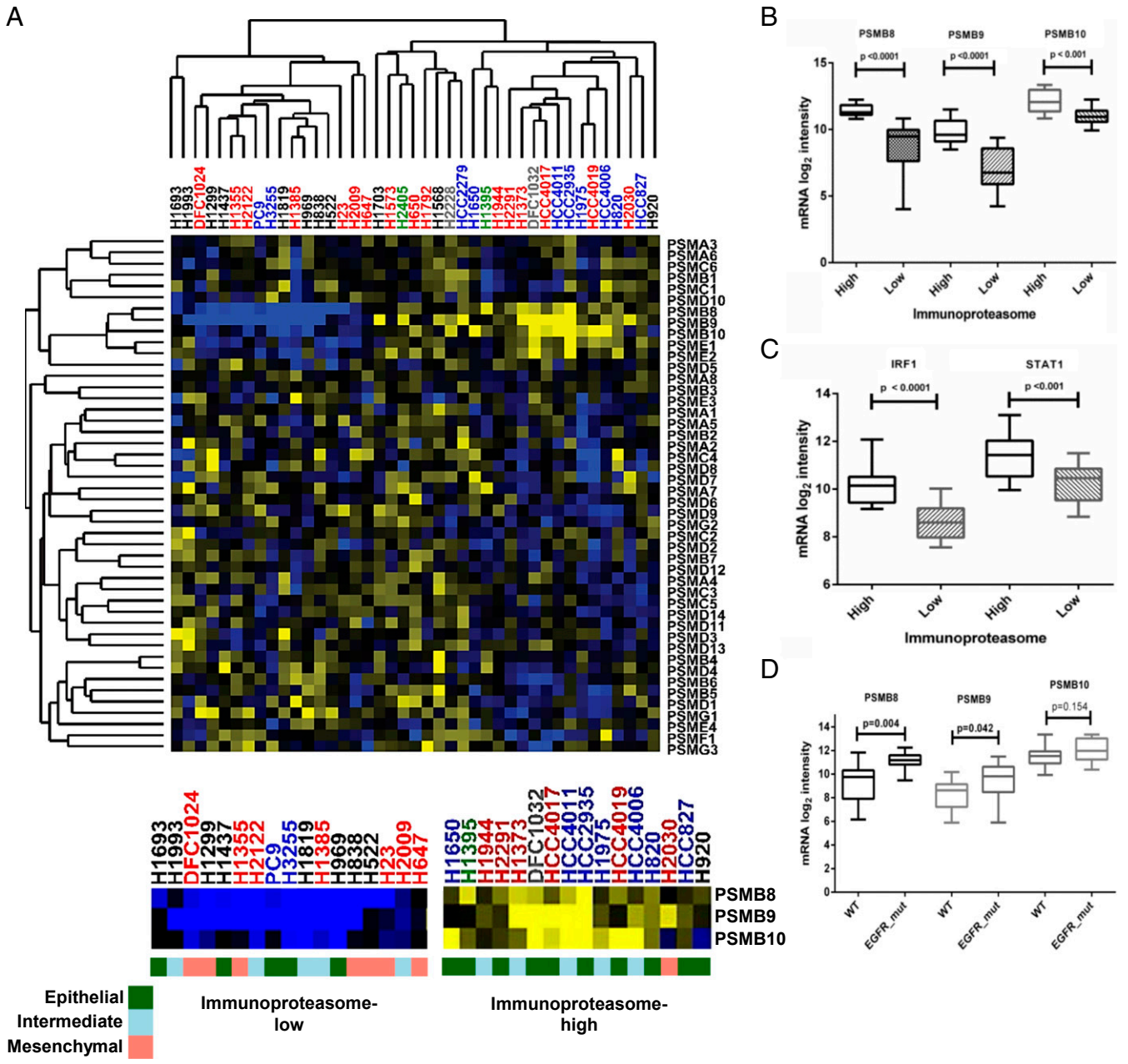

Fig. 1. Proteasome gene expression in lung adenocarcinoma cell lines. (*A*) Heat map plot for proteasome subunits expression among all NSCLC cell lines revealed two clusters with differential gene expression of immunoproteasome subunits. Wild-type, EGFR mutant, Kras mutant, BRAF mutant, and EML-ALK4 mutant cell lines are denoted with black, blue, red, green, and gray labels, respectively. The EMT status of the cell line is indicated by green, light blue, and salmon bars. (*B* and *C*) Significant difference in gene expression of *PSMB8*, *PSMB9*, and *PSMB10* (*B*) and *IRF1* and *STAT1* (*C*) among the cell lines in two clusters. (*D*) EGFR mutants have significantly increased expression of immunoproteasome subunits compared with wild-type cell lines.

expression analysis, exhibited a spindle-shaped mesenchymal-like morphology, whereas immunoproteasome-high lines had a rounded epithelium-like morphology (*SI Appendix*, Fig. S2). We thus hypothesized that differential expression of the immunoproteasome was associated with the epithelial-to-mesenchymal (EMT) status of the cell lines. We used quantitative proteome profiling for both total cell extract (TCE) and the cell surface compartment of representative cell lines from the immunoproteasome-high (DFCI032, HCC2935, H820) and -low (DFCI024, H1299, H838) groups using nanoscale liquid chromatography - tandem mass spectrometry (nano-LC–MS/MS). Differential expression was observed for 655 and 605 proteins on the surface and TCE between the two groups, respectively (Dataset S2). Among these proteins, 366 were up-regulated on the surface of immunoproteasome-low cell lines, including N-cadherin (CDH2) and vimentin ($P = 0.04$ and $P = 0.02$, respectively; t test). HLA class I molecules, cell adhesion-related proteins, and other cell adhesion molecules such as E-cadherin (CDH1), α-catenin, and β-catenin were significantly down-regulated ($P < 0.01$, $P = 0.03$, and $P < 0.01$, respectively; t test). These changes were concordant with gene expression analysis (Datasets S1 and S2). In TCE, 318 proteins were up-regulated in the immunoproteasome-low cell lines, including the aldo-keto reductase family, vimentin, and heat shock proteins, providing additional support for a mesenchymal-like phenotype. Significantly reduced protein expression of PSMB8 ($P = 0.027$),

PSMB9 ($P = 0.005$), and PSMB10 ($P = 0.047$) was also concordant with gene expression findings.

In vitro, wound repair, transwell invasion, and immunoblotting analysis of the EMT markers CDH1 and vimentin revealed increased cell migration, invasion, and reduced immunoproteasome expression, respectively (Fig. 2 *A*–*C*), in immunoproteasome-low cell lines, further confirming a mesenchymal phenotype.

TGFβ stimulation of epithelium-like immunoproteasome-high cell lines (DFCI032, HCC2935, HCC4017, and H820) resulted in markedly decreased expression of the immunoproteasome subunits. Acquisition of a spindle-like morphology with increased level of vimentin and reduced CDH1 expression confirmed TGFβ-induced EMT (Fig. 2 *D* and *E*). Analysis of publicly available data in the GEO database for time-dependent global gene expression during TGFβ-induced EMT yielded concurrent findings of immunoproteasome down-regulation in the lung (GSE17708) and pancreatic adenocarcinoma cell lines (GSE23952). These results ascertained that reduced expression of immunoproteasome is a consequence of EMT.

Immunoproteasome Deficiency Is Associated with Poor Prognosis in NSCLC. To examine the association of immunoproteasome expression with lung cancer histology and prognosis, we performed immunohistochemistry for PSMB8 using a tissue microarray of 218 surgically resected NSCLC tumor specimens (152 adenocarcinomas and 66 squamous cell carcinomas). We detected high PSMB8 expression in the epithelial cells of 96/186 (51.6%) tumor tissues, including 66/115 (57.4%) lung adenocarcinomas and 16/41 (39%) squamous carcinomas without neoadjuvant therapy (Fig. 3 *A* and *B*). Interestingly, high lymphocytic infiltration was observed in many tumors in which PSMB8 expression was below detection levels. PSMB8 expression was also significantly associated with early-stage NSCLC ($P < 0.05$). We also observed a significant positive association between EGFR mutation and PSMB8 expression ($P < 0.05$). No significant association was observed between immunoproteasome subunit expression and sex, age, or smoking status of patients.

Kaplan–Meier survival analysis of patients treated with surgery alone yielded significantly reduced disease-free survival among patients whose tumors had low PSMB8 expression compared with patients with tumors expressing PSMB8 ($P = 0.004$; Fig. 3*C*). PSMB8 levels also emerged as an independent significant prognostic factor for disease-free survival [$P = 0.005$; hazard ratio (HR): 2.5; 95% confidence interval (CI): 1.3–5.0] using Cox multivariate regression analysis after forward stepwise selection of clinicopathological variables (Table 1).

Immunohistochemical (IHC) staining for CDH1 and CDH2 on NSCLC tissue microarrays used for PSMB8 validated that tumors with low PSMB8 expression are often of a mesenchymal or intermediate EMT phenotype. In 74 tumors lacking PSMB8 expression, 34 (45.9%) had detectable levels of the mesenchymal marker CDH2 and/or reduced expression of CDH1 (Fig. 3*A*; $P < 0.001$; Spearman's $\rho = -0.460$), whereas only 5/82 (6.1%) NSCLC tumors positive for PSMB8 expressed detectable levels of CDH2 protein. We further assessed the prognostic value of low PSMB8 expression in NSCLC using the online tool kmplot.com (7). In concordance with IHC findings, Kaplan–Meier survival analysis of data for 1,926 lung cancer patients from 10 datasets revealed decreased survival for patients in the lowest quartile compared with the other three quartiles of PSMB8 gene expression ($P < 0.001$; Fig. 3*D*). Among 982 patients with recorded clinical progression data, time to progression was also significantly reduced for patients in the lowest quartile of PSMB8 expression ($P = 0.0013$; Fig. 3*E*). NSCLC patients with early-stage and low PSMB8 expression also exhibited poor survival rates ($P = 0.006$; *SI Appendix*, Fig. S3*A*), and PSMB8 expression emerged as a significant prognostic factor ($P = 0.0214$; HR: 0.4; 95% CI: 0.19–0.87) in early-stage NSCLC patients using Cox multivariate regression analysis (*SI Appendix*, Fig. S3*B*).

We also examined mRNA expression profiles of immunoproteasome specific subunits in publicly available datasets for NSCLC tissues. A significantly reduced expression of *PSMB8* ($P = 0.009$), *PSMB9* ($P = 0.004$), *HLA-A* ($P = 0.008$), *HLA-B* ($P = 0.035$), and *HLA-C* ($P = 0.028$) was observed in primary lung tumors that recurred after initial therapy compared with primary tumors that did not recur (GSE32863; *SI Appendix*, Fig. S3 *C* and *D*). Analysis of a dataset (GSE2109) containing metastatic and primary lung adenocarcinomas revealed a significantly reduced expression of

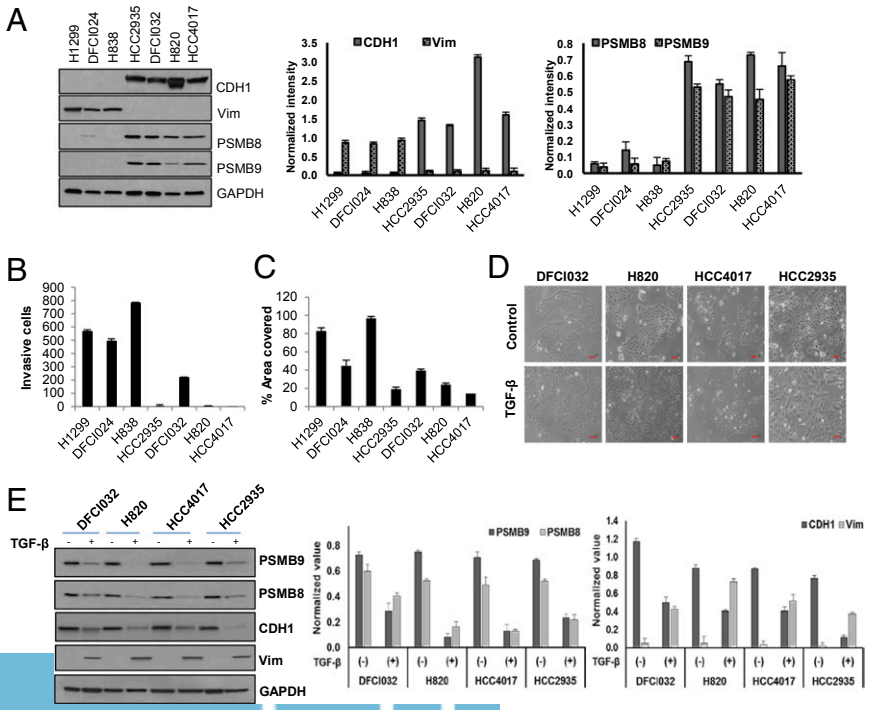

Fig. 2. Characterization of NSCLC cell lines with differential immunoproteasome expression. (*A*) Western blot analysis for EMT markers (CDH1, VIM) and immunoproteasome subunits (PSMB8, PSMB9) in representative NSCLC cell lines. (*B* and *C*) Cells with low immunoproteasome expression were highly invasive (*B*) and had high migration ability and increased motility (*C*) compared with cells with high expression of immunoproteasome subunits. (*D*) Spindle-like morphology was observed in epithelial cell lines treated continuously with TGFβ (10 ng/mL) for 1 wk. (Scale bar, 40 μm.) (*E*) TGFβ treatment induces VIM and decreased CDH1, PSMB8, and PSMB9 expression in epithelial cell lines. Graphs represent comparison of protein level quantification on Western blot after normalization to total protein ($n = 3$; biological replicates). Results are shown as ±SEM. See also *SI Appendix*, Fig. S2.

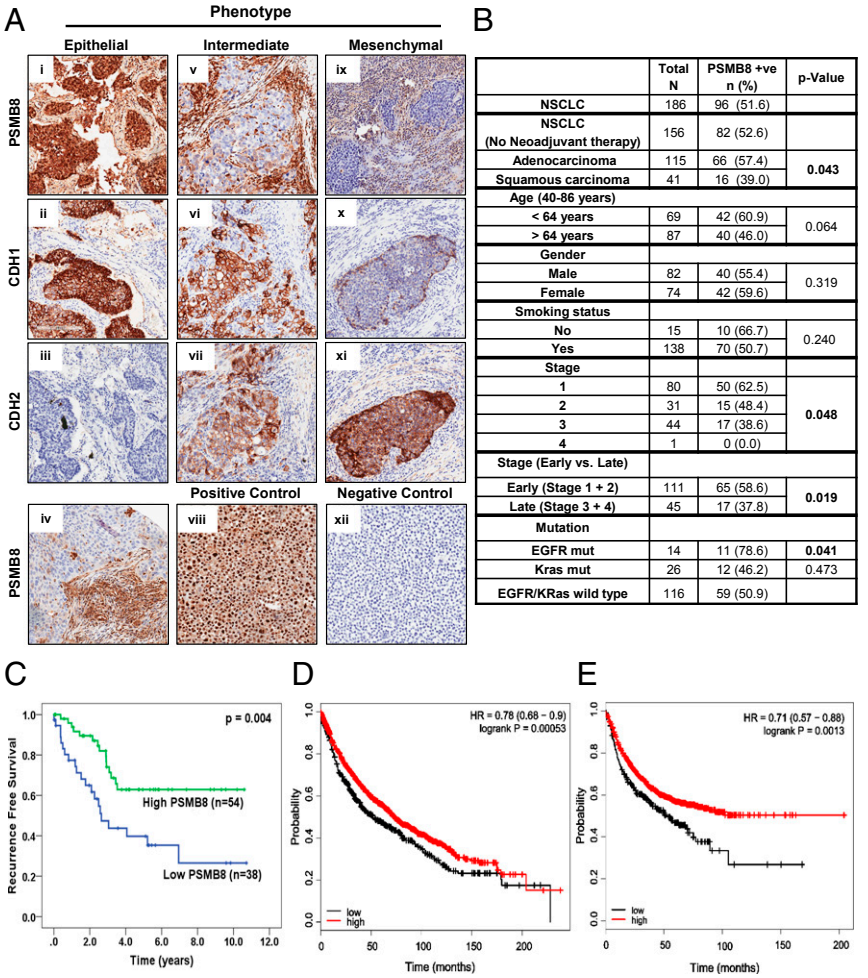

	Total N	PSMB8 +ve n (%)	p-Value
NSCLC	186	96 (51.6)	
NSCLC (No Neoadjuvant therapy)	156	82 (52.6)	
Adenocarcinoma	115	66 (57.4)	**0.043**
Squamous carcinoma	41	16 (39.0)	
Age (40-86 years)			
< 64 years	69	42 (60.9)	0.064
> 64 years	87	40 (46.0)	
Gender			
Male	82	40 (55.4)	0.319
Female	74	42 (59.6)	
Smoking status			
No	15	10 (66.7)	0.240
Yes	138	70 (50.7)	
Stage			
1	80	50 (62.5)	**0.048**
2	31	15 (48.4)	
3	44	17 (38.6)	
4	1	0 (0.0)	
Stage (Early vs. Late)			
Early (Stage 1 + 2)	111	65 (58.6)	**0.019**
Late (Stage 3 + 4)	45	17 (37.8)	
Mutation			
EGFR mut	14	11 (78.6)	**0.041**
Kras mut	26	12 (46.2)	0.473
EGFR/KRas wild type	116	59 (50.9)	

Fig. 3. Tissue microarray analysis. (*A*) IHC analysis of PSMB8 (*i*, *v*, and *ix*), CDH1 (*ii*, *vi*, and *x*), and CDH2 (*iii*, *vii*, and *xi*) in NSCLC tumors revealed lack of PSMB8 expression in cancer cells with low CDH1 and/or increased CDH2 expression. Photomicrographs *i–iii*, *v–vii*, and *ix–xi* represent sections from the same tumor tissues representing epithelial, intermediate, and mesenchymal phenotype as per CDH1 and CDH2 expression status. NSCLC tumor tissue (*iv*) exhibited no expression of PSMB8 in epithelial cells, although a high level of PSMB8 positive lymphocytic infiltration was observed. Cell lines HCC2935 (*viii*) and H1299 (*xii*) served as positive and negative controls, respectively. (Scale bar, 200 μm.) (*B*) Correlation analysis of PSMB8 expression with other clinicopathological features using χ^2 tests. (*C*) Kaplan–Meier analysis for recurrence-free survival in NSCLC. Median recurrence-free survival was 7.5 y in patients immunopositive for PSMB8 compared with 4.6 y in the patients lacking PSMB8 expression. (*D*) Kaplan–Meier survival curves of patients with the lowest quartile of *PSMB8* expression (black line) showed worse survival compared with those in the other three higher quartiles (red line). (*E*) Patients with the lowest quartile of *PSMB8* expression (black line) had a fast clinical progression rate compared with those in the other three quartiles (red line). See also *SI Appendix*, Figs. S1 and S3.

PSMB8 ($P = 0.001$), *PSMB9* ($P < 0.002$), *HLA-A* ($P = 0.042$), *HLA-B* ($P = 0.017$), and *HLA-C* ($P = 0.007$) in metastatic compared with primary tumors (*SI Appendix*, Fig. S3 *E* and *F*).

Immunoproteasome Expression Is Regulated by the mTOR/STAT3 and *MicroRNA-200* Axis. STAT3, a downstream molecule in the mTOR pathway, plays an opposing role to its family member STAT1, a key regulator of immunoproteasome subunits (8). We therefore examined protein expression of these genes between cell lines with epithelial and mesenchymal features. An increase in mTOR and pSTAT3 and a reduction in STAT1 expression were observed in mesenchymal compared with epithelial cells (Fig. 4*A*). We constructed a mathematical model based on experimentally known links between STAT1 and STAT3 (*SI Appendix*, Section 2). STAT1 and STAT3 mutually inhibit the activation of each other, and promote their own activation, whereas *microRNA-200* (*miR-200*) inhibits STAT3 activation indirectly by inhibiting TGFβ (Fig. 4*B*). A typical bifurcation diagram depicts the transition between the different states of STAT1/STAT3 loop as a function of miR-200 (Fig. 4*C*). Our analysis reveals that this double-negative feedback loop between STAT1 and STAT3 can have three steady states that may be linked to EMT and impact immunoproteasome expression. This finding is consistent with our experimental results whereby we observed that mesenchymal cells (low miR-200) usually have high STAT3 expression, whereas epithelial cells (medium to high *miR-200*) can have concomitant intermediate expression of both STAT1 and STAT3 (Fig. 4*D*).

The correlation of STAT3 and STAT1 to components of the immunoproteasome was confirmed in the TCGA lung gene expression dataset (http://cancergenome.nih.gov). In a dataset of 423 tumor specimens, *PSMB8* expression was positively correlated with *STAT1* expression, with a Spearman's $\rho = 0.55$, and loosely anticorrelated with *STAT3* expression, with a Spearman's $\rho = -0.27$. *PSMB8*, *-9*, *-10*, and *IRF1* were all significantly elevated in tumors in the highest vs. lowest quintile of *STAT1* expression and repressed in tumors with the highest vs. lowest quintile of *STAT3* expression (*SI Appendix*, Table S1).

STAT3 can induce DNA methyltransferases (9, 10) and regulate methylation of many genes. Hence, we also analyzed DNA methylation data for *PSMB8*, *PSMB9*, and *IRF1* in the TCGA

Table 1. Univariate and multivariate analyses of disease-free survival of NSCLC patients

	Univariate		Multivariate*	
Variable	HR (95% CI)	*P*	HR (95% CI)	*P*
Sex (male vs. female)	1.48 (0.76–2.86)	0.23	—	0.42
Age (<64 vs. ≥64 y)	1.74 (0.90–3.38)	0.11	—	0.49
Stage (early vs. late)	**2.57 (0.92–7.16)**	**0.01**	—	0.07
Smoking status (yes or no)	0.98 (0.34–2.80)	0.98	—	0.86
Mutational status	0.50 (0.25–1.01)	0.09	—	0.42
PSMB8 (high vs. low)	**0.38 (0.19–0.77)**	**0.003**	**2.58 (1.33–5.00)**	**0.005**

Cox proportional hazards models were used for multivariate analysis. All statistical tests were two-sided. *Variables included in the equation after forward-selection logistic regression. Bold rows indicate significant rows by $P < 0.05$. Dashes indicate components of the multivariate model where no HR was delivered for nonsignificant changes.

dataset. We identified hypermethylation at multiple enhancer CpG sites, associated with a significant inverse correlation with the expression of the corresponding genes (Fig. 4*E* and *SI Appendix*, Table S2). To assess the contribution of methylation to immunoproteasome expression, we treated mesenchymal cell lines (H1299, H838, and DFCI024) with 2 μM of the demethylating agent 5-aza-2′-deoxycytidine (5-aza-dC) for 5 d, which resulted in a significant increase ($P < 0.001$) in mRNA and protein expression of immunoproteasome subunits (Fig. 4 *F* and *G*). Pyrosequencing methylation analysis of promoter and enhancer regions revealed that only enhancer binding sites are highly methylated in mesenchymal cell lines compared with epithelial lines. Methylation was decreased up to 40% in 5-aza-dC treated cell lines compared with the controls (*SI Appendix*, Fig. S3 *A* and *B* and Dataset S3), suggesting epigenetic regulation of the immunoproteasome. Induction of pSTAT1 in mesenchymal cell lines with an mTOR inhibitor (rapamycin, 100 ng/mL) treatment for 5 d also resulted in induction of immunoproteasome subunits (Fig. 5*H*), thus supporting the dual input of STAT3 and STAT1 in regulation of immunoproteasome expression.

HLA Class I-Bound Peptide Repertoire Is Dynamic and Represents the Epithelial vs. Mesenchymal State. We next examined whether reduced immunoproteasome expression led to fewer peptides presented on HLA class I molecules. HLA class I-bound peptides were eluted by mild acid elution from epithelial (DFCI032 and HCC2935) and mesenchymal (DFCI024 and H1299) cell lines and analyzed by nano-LC–MS/MS. We used SYFPEITHI (http://www.syfpeithi.de) and the Immune Epitope Database (http://www.iedb.org) to predict whether these identified peptides could be efficiently bound by HLA class I molecules and which subtype of receptor was bound (Dataset S4). A total of 415 and 400 HLA class I-bound peptides (8- to 11-aa residues) were identified from epithelial cell lines DFCI032 and HCC2935, representing 246 and 247 proteins, respectively. The mesenchymal cell lines H1299 and DFCI024 displayed a marked reduction in the diversity of peptides, with 60 and 98 HLA class I-bound peptides, representing 48 and 84 proteins, respectively. Although the repertoire of HLA class I-bound peptides reflected protein composition of the cell populations investigated, there was substantial variability in protein composition between epithelial and mesenchymal cell lines, suggesting that immunoproteasome expression results in processing and presentation of unique peptides molded by cellular metabolic activity (Fig. 5*C*).

IFNγ Induces the Immunoproteasome and Restores the Immunopeptidome Repertoire in Mesenchymal Cells. IFNγ treatment of mesenchymal cell lines for 24 h restored immunoproteasome subunit expression at a dose as low as 20 ng/mL (Fig. 5*A* and *SI Appendix*, Fig. S5*A*). Enhanced HLA class I expression following IFNγ treatment was also evident by flow cytometry (Fig. 3*B* and *SI Appendix*, Fig. S5*B*). IFNγ treatment of H1299 cells revealed greater than threefold increase in the number of HLA class I-bound peptides ($n = 190$) derived from 126 source proteins (Dataset S5). In DFCI024, a total of 199 HLA class I-bound peptides derived from 139 source proteins were identified with IFNγ treatment, compared with 98 peptides derived from 84 source proteins in untreated cells (Dataset S5). The relative abundance of individual peptides based on MS intensity was also increased in IFNγ-treated compared with nontreated cells (Dataset S6), suggesting that induction of the immunoproteasome has a substantial impact on both the abundance and diversity of HLA class I-bound peptides. The repertoire of proteins from which HLA class I-bound peptides were derived following IFNγ treatment of mesenchymal cells was largely distinct from epithelial cell lines, demonstrating the role of the immunoproteasome on processing and presentation of unique peptides that reflect differences in protein composition between cell types (Fig. 5 *D* and *E*).

Proteins Related to HLA Class I-Bound Peptides Induce Humoral Immunity and Are Overexpressed in NSCLC Patients. Some tumor-associated antigenic (TAA) peptides, when expressed in neoplastic cells, elicit both cell- and humoral-immune responses (11). We hypothesized that HLA-bound peptides identified by mass spectrometry were also derived from aberrantly expressed or processed proteins that displayed immunogenic properties reflected in the induction of autoantibodies. Arrays spotted with 9,400 recombinant proteins were hybridized each with prediagnostic plasmas from 25 newly diagnosed NSCLC cases and an equal number of controls matched for age and date of blood collection. A total of 158 and 162 arrayed recombinants were represented as HLA class I-bound peptides in analysis of DFCI032 and HCC2935 cells, respectively. Remarkably, 116/158 and 128/162 proteins from DFCI032 and HCC2935 cells, respectively, were found to be associated with autoantibodies among NSCLC subjects (Dataset S7). Autoantibodies were also identified against 72/91 and 78/106 protein sources of HLA class I-bound peptides presented on the surface of IFNγ-treated H1299 and DFCI024 cells, respectively (Dataset S7). Humoral immunity was observed against a subset of 13 proteins (case vs. control, $P < 0.05$; Wilcoxon rank-sum test) that had corresponding HLA-bound peptides in common between the two epithelial cell lines and IFNγ-treated mesenchymal cell lines (*SI Appendix*, Table S3).

TAA peptides are often aberrantly expressed in cancer compared with normal tissues. We evaluated NSCLC tumors in the TCGA dataset for expression of genes encoding HLA class I-bound peptides. Genes encoding proteins for which HLA class I-bound peptides were identified in NSCLC cell lines generally exhibited significantly increased expression levels in tumor tissues compared with adjacent nontumor tissue, including 12 of 17 genes that were found in common between epithelial and IFNγ-treated mesenchymal cell lines (*SI Appendix*, Table S4). Based on the BioGPS dataset, most of these genes were expressed at low levels in normal tissues (12). HLA class I-bound peptides for two cancer testis antigens, acrosin binding protein (ACRBP, or OY-Tes-1) and catenin alpha-2 (CTNNA2, or CT 114) were also detected in the epithelial lines.

HLA Class I-Bound Peptides Are Recognized by $CD8^+$ T Cells, Resulting in Cell Killing. Epithelial cell lines DFCI032 and HCC2935 express HLAA*02:01 (*SI Appendix*, Section 3), which occurs in ∼50% of Caucasians. HLA class I-bound peptides identified in both cell lines were tested for HLA-A*02:01–binding properties using the publicly available algorithm, HLArestrictor (13). Mesenchymal cell lines tested negative for HLA-A*02. HLA-A*24:02, encoded by H1299 and DFCI024, was selected for analysis, because of its high global frequency. Peptides from mesenchymal

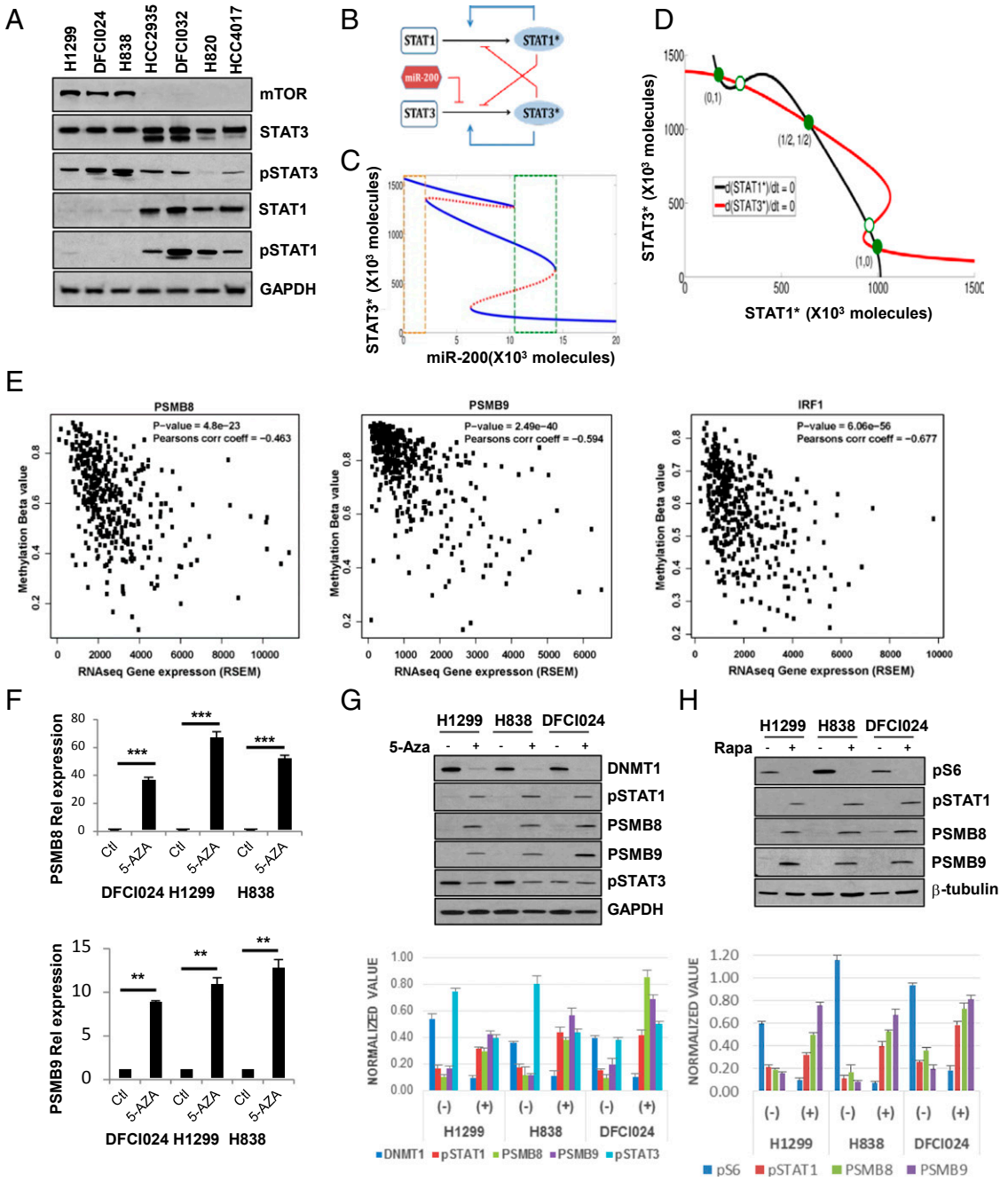

Fig. 4. Regulatory control of immunoproteasome proteins. (*A*) STAT1 and mTOR are highly expressed in epithelial and mesenchymal cell lines, respectively, with no change in STAT3 levels. (*B*) Regulatory network for STAT1–STAT3: active forms STAT1* and STAT3* mutually inhibit each other's activation and promote self-activation. miR-200 inhibits activation of STAT3. (*C*) Bifurcation of STAT3* levels driven by miR-200. For low values of miR-200, only one state exists: STAT3* high levels (orange dotted rectangle). For high values of miR-200, either of two states can exist: STAT3* medium (and STAT1* medium) or STAT3* low (and STAT1* high) (green dotted rectangle). Solid blue lines indicate stable fixed points, whereas red dotted lines indicate unstable fixed points. (*D*) Nullclines and states corresponding to the network in *B*. The STAT1*–STAT3* network is tri-stable, with three states denoted by (0,1), (1,0), and (1/2,1/2). Green solid squares and hollow circles denote stable and unstable fixed points, respectively. (*E*) Gene expression and methylation data obtained from the TCGA lung dataset revealed an inverse correlation for PSMB8, PSMB9, and IRF1. (*F* and *G*) Quantitative RT-PCR (*F*) and immunoblot (*G*) analyses indicate induction of PSMB8 and PSMB9 following 5-aza-dC (2 μM) treatment for 5 d in mesenchymal cells (**$P < 0.01$, ***$P < 0.001$; *t* test). pSTAT1 expression was induced with decrease in DNMT1 and no remarkable change in pSTAT3 protein levels after treatment. (*H*) Rapamycin (100 ng/mL) treatment for 5 d induced immunoproteasome subunit expression via pSTAT1 in mesenchymal cells. Graphs represent protein level quantification on Western blot after normalization to total protein ($n = 2$; biological replicates). Results are shown as ±SEM. See also *SI Appendix*, Section 2 and Fig. S4.

cells were categorized based on their occurrence as follows: peptides identified only after exposure to IFNγ (+IFNγ), peptides expressed only in cells without IFNγ (−IFNγ), or peptides common in cells with and without IFNγ treatment (±IFNγ). Peptides from epithelial and mesenchymal cell lines predicted by HLArestrictor to bind with <500 nM IC_{50} nM to HLA-A*02 or HLAA*24, respectively, were selected for further analysis (*SI Appendix*, Table S5).

To determine whether the identified HLA I-bound peptides could be recognized by T cells, we used the established peptide–T2

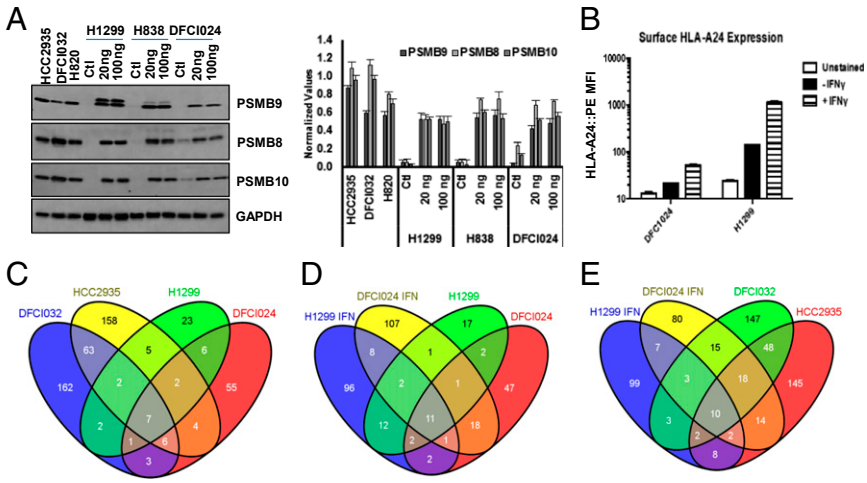

Fig. 5. Effect of IFNγ on immunoproteasome expression. (*A*) IFNγ treatment induced immunoproteasome expression in mesenchymal cells. Epithelial cell lines were used as positive controls. The graph represents protein quantification on Western blot after normalization to total protein ($n = 3$; biological replicates). (*B*) Specific staining for HLA-A24 revealed increased expression on mesenchymal cells with IFNγ compared with controls. Bar graphs display the average mean fluorescence intensity (MFI) ± SD ($n = 3$; technical replicates). (*C*–*E*) Venn diagrams for number of proteins degraded and presented as HLA I-bound peptides in epithelial compared with mesenchymal cell lines (*C*) and in IFNγ-treated mesenchymal cell lines compared with untreated mesenchymal (*D*) and compared with epithelial (*E*) cell lines. See also *SI Appendix*, Fig. S5.

binding assay (14). We performed peptide titration and confirmed peptide binding to HLA-A*02:01, with the HLA-A*02–binding nonamer PR1 (VLQELNVTV) serving as a positive control (15) (Fig. 6*A*). Peripheral blood mononuclear cells matched for HLA were stained with tetramers to detect circulating peptide-specific $CD8^+$ cytotoxic T lymphocytes (CTLs) (Fig. 6*B*). The functionality of CTLs was assessed with cell-mediated cytotoxicity assays after expanding T cells ex vivo with peptide-pulsed antigen-representing cells (APCs) (Fig. 6 *C* and *D*). Target cells pulsed with an irrelevant peptide generated from HIV were used as negative controls. Of the HLA-A2–specific peptides found on epithelial cell lines, VVLDDKDYFL, derived from heat shock protein, mitochondrial (HSPE1), displayed the highest binding affinity to HLA-A2 (Fig. 6*A*) as well as the highest CTL-mediated specific killing of a peptide-pulsed target lymphoblastic cell line (LCL) (Fig. 6*C*). Three other HLA-A2–specific peptides, FMILPVGAANF, PILYRPVAVAL, and FTADHPFLF, derived from α-enolase (ENO1), pyruvate kinase (PKM), and leukocyte elastase inhibitor (SERPINB1), respectively, also stimulated CTL-mediated killing at various effector:target ratios.

Peptides found only after IFNγ induction of the immunoproteasome in mesenchymal cells and with predicted HLA-A24–binding properties also induced peptide-specific cytotoxicity against a pulsed LCL at all effector:target ratios examined (Fig. 6*D*, blue). Epitopes of those two peptides, KFIDTTSKF and IFILPSAF, are contained within the 60S ribosomal protein L3 (RPL3) and the sodium-coupled neutral amino acid transporter 2 (SLC38A2), respectively. Peptide-specific cytotoxicity was also only observed against NFLLQQNFDED, derived from UV excision repair protein RAD23 homolog B (RAD23B), presented by mesenchymal cells ±IFNγ (Fig. 6*D*, red). In contrast, peptide-specific cytotoxicity was significantly reduced for peptides from untreated mesenchymal cells (Fig. 6*D*, green). However, some limited cytotoxicity was observed at lower effector:target ratios against AANFLLQQNF, an epitope with sequence overlap with the peptide NFLLQQNFDED from mesenchymal cells ±IFNγ.

To elucidate whether CTLs expanded against immunogenic peptides identified following IFNγ treatment could result in lung cancer cell killing, CTLs were expanded in vitro against an HLA-A24–bound peptide derived from RPL3, identified in mesenchymal cells +IFNγ. When challenged against H1299 +IFNγ, a significantly increased cell lysis was observed (Fig. 6*E*). Similar findings were obtained with a peptide derived from RAD23B, observed in mesenchymal cells ±IFNγ (Fig. 6*F*). These observations indicate that circulating CTLs are capable of recognizing and eliminating lung cancer cells presenting endogenous peptides identified in our study.

Discussion

T cell-mediated immune tumor suppression is a complex process with numerous requirements (16, 17). One such requirement is antigen processing by the immunoproteasome and presentation through HLA class I surface molecules expressed on tumor cells. In nonmalignant cells, protein processing through the immunoproteasome is a feature of adaptive immune response induced by inflammatory cytokines (18, 19). Recently, up-regulated expression of immunoproteasome subunits in solid tumors has been reported, with preserved basal level in normal epithelium. This finding is notable because the immunoproteasome was previously thought to be constitutively expressed only in dendritic cells, macrophages, or activated lymphocytes (20, 21). We observed substantial heterogeneity in mRNA and protein expression of immunoproteasome-related genes among NSCLC cell lines. Interestingly, epithelial cell lines displayed constitutive expression of the immunoproteasome, which may be attributed to signaling through the EGFR, IL6, or PDGF pathways (22). These signaling pathways are known to enhance STAT1 levels, which in turn can regulate IFN related genes. Reduced expression of immunoproteasome subunits was observed in mesenchymal cell lines compared with their epithelial counterparts at the RNA and protein levels. We found that EMT induction in epithelial cell lines resulted in a markedly decreased expression of immunoproteasome subunits. TGFβ-induced EMT was also associated with a significant decrease in immunoproteasome expression. Given the association between EMT and immune evasion and poor outcome and metastasis (23, 24), we hypothesized that suppression of the immunoproteasome in mesenchymal cells is a mechanism of escape from immune surveillance. IHC analysis of PSMB8 and known EMT markers on tissue microarrays also supported a significant association between low immunoproteasome expression and a mesenchymal or intermediate EMT phenotype in NSCLC patients. Tumors possessing intermediate EMT phenotypes maintain plasticity between an epithelial and mesenchymal

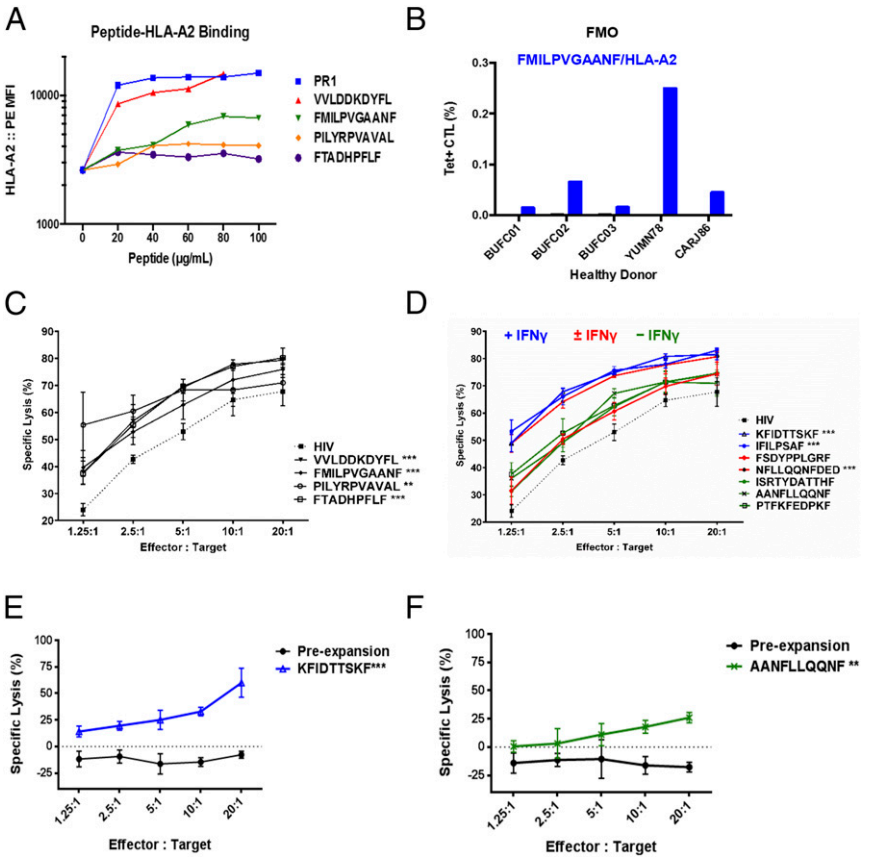

Fig. 6. Endogenous peptides are recognized by CTLs. (*A*) HLA class I-bound peptides from epithelial cells display A2-binding characteristics. T2 cells were used to detect surface HLA-A2 molecules stabilized by peptides at the indicated dose. (*B*) Frequency of endogenous CTLs from five different $A2^+$ donors specific for representative FMILPVGAANF/HLA-A2 complexes were detected by MHC class I tetramer staining. CTLs lacking tetramer staining (FMO) served as a negative control. (*C* and *D*) CTLs expanded against the indicated peptides displayed by HLA-$A2^+$ epithelial (*C*) and mesenchymal (*D*) NSCLC cell lines are functional and lyse peptide-pulsed target cells (LCL) (HLA-$A2^+$, -$A24^+$). $^{***}P < 0.001$; $^{**}P < 0.01$. Bars represent mean specific lysis ± SD from three technical replicates at different effector:target ratios. (*E* and *F*) Cytotoxicity of H1299 cells was enhanced following expansion of CTL in vitro against an APC (HLA-A24–positive LCL) pulsed with peptide discovered on H1299 cells with treatment (+IFNγ) (KFIDTTSKF, blue line) (*E*) or without IFNγ treatment (−IFNγ) (AANFLLQQNF, green line) (*F*). Two-way ANOVA test used ($^{***}P < 0.001$; $^{**}P < 0.01$) and mean cytotoxicity from three or more individual donors are displayed; error bars indicate ±SD.

phenotype, which may suggest that lower immunoproteasome expression occurs before cells become locked in a mesenchymal state (25–27). A better prognosis in NSCLC patients was significantly associated with increased immunoproteasome expression, potentially attributable to IFNγ secreted by T lymphocytes infiltrating the tumor. However, we also found tumors infiltrated with T lymphocytes without any expression of the immunoproteasome (Fig. 2*A*), suggesting that immunoproteasome expression may be an independent prognostic factor as per our multivariate analysis. EMT can profoundly alter the susceptibility of cancer cells to T-cell-mediated immune surveillance (28, 29) which may be partially mediated by loss of the immunoproteasome.

Infiltrating lymphocytes secrete numerous cytokines like IFNγ, IL-6, TGFβ, and TNFα. All of these cytokines are known to impact the transcriptional machinery in a cell, including activation of the PI3K/AKT/mTOR pathway. STAT3, the downstream effector of the mTOR pathway, acts as an antagonist for STAT1, a key regulator of immunoproteasome and antigen-presenting machinery (8, 30). STAT3 signaling is required for TGFβ-induced EMT in lung cancer cells (31) and plays an opposite role to STAT1, which promotes antitumor effects and immunosurveillance (32, 33). We propose a mathematical model that explains coupling between the STAT1–STAT3 feedback loop to the *miR-200*/ZEB loop and how these networks together lead to high STAT3 and low STAT1 expression in mesenchymal cancer cells (*SI Appendix*, Section 2), thus leading to differential expression of the immunoproteasome. Additionally, our model accounts for balanced expression of STAT1 and STAT3 in epithelial cancer cells, regulating immunoproteasome expression (*SI Appendix*, Fig. S6).

STAT3, IL-6, and TGFβ can also induce DNA methyltransferases, which may contribute to down-regulation of the STAT1, HLA class I, and immunoproteasome-related genes (9, 34, 35). We provide evidence that modulating STAT3 activity either by treatment with a demethylating agent or the mTOR inhibitor rapamycin increased STAT1 phosphorylation and immunoproteasome subunit expression. Our analysis of lung cancer patients in the TCGA database suggested a significant inverse correlation of gene expression and DNA methylation for immunoproteasome related genes. Pyrosequencing analysis of NSCLC cell lines revealed methylation at enhancer binding sites of immunoproteasome subunit genes that correlated with repressed expression in mesenchymal cell lines.

IFNγ is known to induce the immunoproteasome and has numerous antitumor effects (36). Treatment of mesenchymal cell lines with IFNγ led to up-regulation of the immunoproteasome and induces pSTAT1. IFNγ plays key roles in tumor immune surveillance, can act as an epigenetic modifier to up-regulate gene expression, and has been investigated as a treatment for various cancers (37, 38). As we have shown that immunoproteasome downregulation may occur through an epigenetic or a STAT1/STAT3 dependent mechanism, IFNγ treatment may act at multiple points to overcome this inhibition.

Peptide products of proteins with a high turnover rate are major constituents of the immunopeptidome of cancer cells (39). These peptides play a role in adaptive immunity against tumors through their presentation to $CD8^+$ T cells. We analyzed the repertoire of HLA class I-bound peptides from epithelial and mesenchymal cell lines. Mesenchymal cells with IFNγ-induced immunoproteasome expression showed a marked increase in HLA class I-bound peptides. Using a proteomic-based approach, we identified HLA class I-bound peptides from epithelial, mesenchymal, and IFNγ-treated mesenchymal cells and demonstrated that identified HLA class I-bound peptides are functional, resulting in lung cancer cell killing. Identified functional peptides include those derived from proteins such as PKM2 that have previously described roles in tumor proliferation and survival, as well as proteins such as SERPBINB1, which is part of a previously described lung cancer proteomic signature (40, 41).

Analysis of the TCGA lung dataset revealed that at least 75% of the proteins presented as HLA class I-bound peptides are upregulated in lung cancer compared with normal lung tissue. Thirteen of these proteins were presented as peptides in both epithelial and IFNγ-treated mesenchymal cells. Expression of these proteins is largely restricted to tumor cells. This set includes STIP1, previously proposed as a cancer biomarker (42, 43), S100A11, which is associated with invasion and metastasis (44, 45), and two cancer testis antigens, OY-Tes-1 and CT 114, not previously associated with NSCLC. A recent article demonstrated that T-cell reactivity to self-antigens are "pruned, but not eliminated" in healthy individuals (46), contrary to the dogma that self-reactive T cells are completely eliminated. Hence, it could be feasible to use cancer-specific endogenous MHC I peptides generated from proteins overexpressed in tumors as immunotherapeutic targets. Additionally, in support of the immunogenic nature of proteins for which we identified HLA class I-bound peptides, we observed an autoantibody response against several of these proteins in plasma samples from NSCLC patients collected before diagnosis compared with matched noncancer controls.

Our findings suggest an alternative therapeutic strategy consisting of CTL-based immunotherapy combined with induction of the immunoproteasome via IFNγ, rapamycin, or a demethylating agent to target cells that have undergone EMT. The restricted HLA class I-bound antigen repertoire inherent to tumor cells with a mesenchymal phenotype may thus be circumvented through induction of the immunoproteasome or through identifying and targeting antigens not dependent on the immunoproteasome for their presentation. As with immune checkpoint inhibition, induction of the immunoproteasome in cells that have undergone EMT could serve as a potent tool to counteract the immune evasion phenotype correlated with poor outcome and metastasis.

Experimental Procedures

Detailed descriptions are provided in the *SI Appendix*.

Cell Culture and Drug Treatment. NSCLC cell lines from initial authenticated cell passages, free from mycoplasma, were grown in Roswell Park Memorial Institute (RPMI)-1640 with 10% (vol/vol) FBS and 1% penicillin/streptomycin mixture. For SILAC labeling, cells were grown for seven passages in RPMI-1640 supplemented with [^{13}C]lysine and 10% (vol/vol) dialyzed FBS according to the standard protocol (47). Details are given in *SI Appendix*, Section 4.

Tumor Tissue Samples and IHC Analysis. The tissue microarrays used in this study consisted of 218 surgically resected NSCLC tumor specimens collected under an MD Anderson Cancer Center institutional review board-approved protocol. Immunohistochemistry was performed using a Leica Bond Max automated stainer (Leica Biosystems) (4, 48). The validated primary antibodies used were PSMB8 (LMP7, 1:200, mouse monoclonal; Abcam ab58094), CDH1 (prediluted, mouse monoclonal clone NCH-38; Dako ISO59), and CDH2 (1:50, rabbit monoclonal clone D4R1H; Cell Signaling Technology 13116). Formalin-fixed paraffin-embedded cell pellets from Western blot-tested cell lines HCC2935 (positive) and H1299 (negative) were used as controls for PSMB8. Human lung adenocarcinoma for CDH1 and human normal fallopian tube for CDH2 were used as a positive control. Also, a nonprimary antibody control was used as an additional control. IHC samples were quality-checked and evaluated by two pathologists (H.L. and J.R.-C.) who were blinded to the study and clinical outcome of the patients. The scorers did not have prior knowledge of the local tumor burden, lymphonodular spread, and grading of the tissue samples. For protein expression, sections were scored as positive if >10% epithelial cells showed immunopositivity in the cytoplasm or nucleus for PSMB8 and membrane for CDH1 and CDH2. The IHC scoring system used was H-score, which evaluates intensity (0–3) and percentage of positive tumor cells (0–100), with a final scoring ranging from 0 to 300. The highest score among replicates (three core biopsies) was considered as representative. A cutoff score of 100 was used as a criterion for PSMB8 positivity. The scoring by the observers was discrepant in about 5% cases, and a consensus on the final result was reached by reevaluation of these slides and discussion.

Quantitative PCR, Western Blot, and DNA Bisulfite-Pyrosequencing Methylation Analysis. Standard protocols were used; details are given in *SI Appendix*, Sections 5–7.

Wound-Healing, Migration, and Invasion Assays. Standard protocols were used; details are given in *SI Appendix*, Section 9.

Mathematical Modeling for STAT1–STAT3 Interaction Circuit. A mathematical model based on experimentally known links between STAT1 and STAT3 was constructed to explore the possible relationship between these two proteins and hence their effect on the immunoproteasome complex. The MATLAB continuation method MATCONT was used to calculate the nullclines and bifurcations. Model formulation and all model parameters can be found in *SI Appendix*, Section 2.

Mass Spectrometric Analysis. Proteomic analysis was performed as previously described (49). Detailed methods for mass spectrometric analysis can be found in *SI Appendix*, Section 11.

HLA-Bound Peptide Extraction and MS Analysis. HLA-bound peptides were eluted from 5×10^8 cells of epithelial (HCC2935, DFCI032) and mesenchymal (H1299, DFCI024) cell lines as previously described (50). H1299, DFCI024 cell lines were incubated with or without 20 ng/mL IFNγ for 24 h before elution of HLA-bound peptides. In brief, 4 mL of citrate-phosphate buffer at pH 3.3 (0.131 M citric acid/0.066 M Na_2HPO_4, NaCl 150 mM) containing a protease inhibitor mixture and phosphatase inhibitors was added to each dish. Cells were scraped gently from the plate and pooled together and resuspended by gentle pipetting for 1 min to denature HLA-peptide complexes. Cell suspensions were then pelleted, and the resulting supernatant was isolated. Peptides were then passed through ultrafiltration devices (3-kDa cut off, Amicon Ultra; Millipore) to isolate peptides from β2m proteins. Peptides obtained after acid elution were desalted and separated using an off-line 1100 series HPLC system (Shimadzu) with reversed-phase column (4.6-mm internal diameter × 150-mm length; Column Technology). Peptides were fractionated with a 41-min elution program at a flow rate of 2.1 mL/min: 0–2% B (0–5 min), 2–35% B (5–30 min), 35–50% B (30–33 min), 50–95% B (33–35 min), 95% B (35–37 min), 95–2% B (37–37.5 min), 2% B (37.5–41 min). Mobile phase A: 5% acetonitrile, 95% H_2O, 0.1% trifluoroacetic acid (TFA); Mobile phase B: 5% H_2O, 95% acetonitrile, 0.1% TFA. The fractionated peptides were collected in 96 consecutive fractions, lyophilized, and subsequently resuspended in 50 μL of 1% TFA after pooling into 12 pools of consecutively eluting fractions and analyzed by nano-LC–MS/MS using LTQ-Orbitrap Elite mass spectrometer connected with Easy-nLC 1000 (Fisher Scientific). Full mass spectra were acquired at a resolving power of 60,000 (at *m/z* 400), and collision-induced dissociation tandem mass spectra were acquired in data-dependent mode. For peptide identification, database searches were performed against the updated 2013 UniProtKB; 20,224 entries with a mass precursor tolerance of ±20 ppm and a fragment tolerance of ±0.7 Da were found. Search results were filtered based on an false-discovery rate (FDR) of 0.05 with Proteome Discoverer and subsequently filtered using an HLA motif filter (SYFPEITHI and IEDB) based on the predicted human HLA I allele motifs (*SI Appendix*, Section 3). Raw data files were converted to peptide maps comprising *m/z* values, charge state, retention time, and intensity for all detected ions above a threshold of 5,000 counts using Proteome Discoverer software (version 1.4; Fisher Scientific). Predicted HLA class I-bound peptides were further inspected for mass accuracy, and MS/MS spectra were validated manually. All predicted HLA class I peptides were searched using the NCBI BLASTp algorithm against the human non-redundant protein database to identify the peptides' corresponding source.

Data Analysis. Detailed methods for data analysis can be found in *SI Appendix*, Sections 6 and 12.

Cell-Mediated Cytotoxicity Assays. Target LCL were pulsed with 100 μg/mL of the indicated peptide overnight before cytotoxicity assays. HIV GAG nonamer (Bio-Synthesis) served as an irrelevant control peptide. Target cells were labeled with 5 μg of Calcein acetoxymethyl ester (AM) (354217; BD Biosciences) for 15 min, and excess Calcein AM was removed by repeat washes. CTL and target cells were incubated for 4 h at 37 °C in a humidified incubator at various effector:target ratios. Trypan blue was used as a fluorescence quencher, and fluorescence of live target cells was determined using a CytoFluor II plate reader (PerSeptive Biosystems). Percentage specific cytotoxicity was calculated according to the following equation: $(1 - [\text{fluorescence}_{\text{target + effector}} - \text{fluorescence}_{\text{medium}}]/[\text{fluorescence}_{\text{target alone}} - \text{fluorescence}_{\text{medium}}]) \times 100$ (15). Experimental details are given in *SI Appendix*, Sections 13–15.

Statistical Analysis. The IHC data were subjected to statistical analysis using the SPSS 22.0 software. The relationships between PSMB8 expression and clinicopathological parameters were tested using χ^2 and Fisher's exact tests. Two-sided P values were calculated, and $P < 0.05$ was considered to be significant. Prognostic significance of PSMB8 expression was assessed by Kaplan–Meier survival and multivariate Cox proportional hazards regression analysis. Univariate and multivariate analysis were used to assess the influence of clinical variables on survival. Gene expression data were normally distributed and are presented as means ± SEM. Differences between groups were evaluated using a two-tailed t test. We considered a two-tailed P value less than 0.05 to indicate statistical significance.

ACKNOWLEDGMENTS. We are thank the personnel of the University of Texas M. D. Anderson Cancer Center Sequencing Facility and Flow Cytometry and Cell Sorting Core Facility for providing assistance. Funding support was provided by the Department of Defense (DOD) Congressionally Mandated Lung Cancer Research Program, the National Cancer Institute Early Detection Program, the Canary Foundation, the Leukemia & Lymphoma Society Translational Research Program Grant (6030-12), National Institutes of Health (NIH) SPORE Grant P50 CA100632, and NIH Research Program Project Grants P01 CA049639 and P01 CA148600 (to J.J.M.). Support was also provided by NIH Training Program in Cancer Immunobiology Grant T32 CA009598 (to H.L.P.).

1. Ciechanover A, Stanhill A (2014) The complexity of recognition of ubiquitinated substrates by the 26S proteasome. *Biochim Biophys Acta* 1843(1):86–96.
2. Kuhn DJ, et al. (2009) Targeted inhibition of the immunoproteasome is a potent strategy against models of multiple myeloma that overcomes resistance to conventional drugs and nonspecific proteasome inhibitors. *Blood* 113(19):4667–4676.
3. Chapiro J, et al. (2006) Destructive cleavage of antigenic peptides either by the immunoproteasome or by the standard proteasome results in differential antigen presentation. *J Immunol* 176(2):1053–1061.
4. Taguchi A, et al. (2014) A search for novel cancer/testis antigens in lung cancer identifies VCX/Y genes, expanding the repertoire of potential immunotherapeutic targets. *Cancer Res* 74(17):4694–4705.
5. Selamat SA, et al. (2012) Genome-scale analysis of DNA methylation in lung adenocarcinoma and integration with mRNA expression. *Genome Res* 22(7):1197–1211.
6. Yamauchi M, et al. (2011) N-cadherin expression is a potential survival mechanism of gefitinib-resistant lung cancer cells. *Am J Cancer Res* 1(7):823–833.
7. Győrffy B, Surowiak P, Budczies J, Lánczky A (2013) Online survival analysis software to assess the prognostic value of biomarkers using transcriptomic data in non-small-cell lung cancer. *PLoS One* 8(12):e82241.
8. Avalle L, Pensa S, Regis G, Novelli F, Poli V (2012) STAT1 and STAT3 in tumorigenesis: A matter of balance. *JAK-STAT* 1(2):65–72.
9. Zhang Q, et al. (2006) STAT3 induces transcription of the DNA methyltransferase 1 gene (DNMT1) in malignant T lymphocytes. *Blood* 108(3):1058–1064.
10. Feng J, et al. (2010) Dnmt1 and Dnmt3a maintain DNA methylation and regulate synaptic function in adult forebrain neurons. *Nat Neurosci* 13(4):423–430.
11. Jäger E, et al. (1998) Simultaneous humoral and cellular immune response against cancer-testis antigen NY-ESO-1: Definition of human histocompatibility leukocyte antigen (HLA)-A2-binding peptide epitopes. *J Exp Med* 187(2):265–270.
12. Su AI, et al. (2004) A gene atlas of the mouse and human protein-encoding transcriptomes. *Proc Natl Acad Sci USA* 101(16):6062–6067.
13. Erup Larsen M, et al. (2011) HLArestrictor–A tool for patient-specific predictions of HLA restriction elements and optimal epitopes within peptides. *Immunogenetics* 63(1):43–55.
14. Oh S, et al. (2004) Human CTLs to wild-type and enhanced epitopes of a novel prostate and breast tumor-associated protein, TARP, lyse human breast cancer cells. *Cancer Res* 64(7):2610–2618.
15. Molldrem JJ, et al. (2000) Evidence that specific T lymphocytes may participate in the elimination of chronic myelogenous leukemia. *Nat Med* 6(9):1018–1023.
16. Melief CJ, Finn OJ (2011) Cancer immunology. *Curr Opin Immunol* 23(2):234–236.
17. Rosenberg SA, Yang JC, Restifo NP (2004) Cancer immunotherapy: Moving beyond current vaccines. *Nat Med* 10(9):909–915.
18. Ebstein F, Kloetzel PM, Krüger E, Seifert U (2012) Emerging roles of immunoproteasomes beyond MHC class I antigen processing. *Cell Mol Life Sci* 69(15):2543–2558.
19. Krüger E, Kloetzel PM (2012) Immunoproteasomes at the interface of innate and adaptive immune responses: Two faces of one enzyme. *Curr Opin Immunol* 24(1):77–83.
20. Keller IE, et al. (2015) Regulation of immunoproteasome function in the lung. *Sci Rep* 5:10230.
21. Wehenkel M, et al. (2012) A selective inhibitor of the immunoproteasome subunit LMP2 induces apoptosis in PC-3 cells and suppresses tumour growth in nude mice. *Br J Cancer* 107(1):53–62.
22. Calò V, et al. (2003) STAT proteins: From normal control of cellular events to tumorigenesis. *J Cell Physiol* 197(2):157–168.
23. Houthuijzen JM, Daenen LG, Roodhart JM, Voest EE (2012) The role of mesenchymal stem cells in anti-cancer drug resistance and tumour progression. *Br J Cancer* 106(12):1901–1906.
24. Kitamura T, Qian BZ, Pollard JW (2015) Immune cell promotion of metastasis. *Nat Rev Immunol* 15(2):73–86.
25. Tan TZ, et al. (2014) Epithelial-mesenchymal transition spectrum quantification and its efficacy in deciphering survival and drug responses of cancer patients. *EMBO Mol Med* 6(10):1279–1293.
26. Lu M, Jolly MK, Levine H, Onuchic JN, Ben-Jacob E (2013) MicroRNA-based regulation of epithelial-hybrid-mesenchymal fate determination. *Proc Natl Acad Sci USA* 110(45):18144–18149.
27. Jolly MK, et al. (2015) Implications of the hybrid epithelial/mesenchymal phenotype in metastasis. *Front Oncol* 5:155.
28. Akalay I, et al. (2013) Epithelial-to-mesenchymal transition and autophagy induction in breast carcinoma promote escape from T-cell-mediated lysis. *Cancer Res* 73(8):2418–2427.
29. Chouaib S, Janji B, Tittarelli A, Eggermont A, Thiery JP (2014) Tumor plasticity interferes with anti-tumor immunity. *Crit Rev Immunol* 34(2):91–102.
30. Zhou J, et al. (2007) Activation of the PTEN/mTOR/STAT3 pathway in breast cancer stem-like cells is required for viability and maintenance. *Proc Natl Acad Sci USA* 104(41):16158–16163.
31. Liu RY, et al. (2014) JAK/STAT3 signaling is required for TGF-β-induced epithelial-mesenchymal transition in lung cancer cells. *Int J Oncol* 44(5):1643–1651.
32. Brucet M, Marqués L, Sebastián C, Lloberas J, Celada A (2004) Regulation of murine Tap1 and Lmp2 genes in macrophages by interferon gamma is mediated by STAT1 and IRF-1. *Genes Immun* 5(1):26–35.
33. Huang S, Bucana CD, Van Arsdall M, Fidler IJ (2002) Stat1 negatively regulates angiogenesis, tumorigenicity and metastasis of tumor cells. *Oncogene* 21(16):2504–2512.
34. Li Y, et al. (2012) IL-6-induced DNMT1 activity mediates SOCS3 promoter hypermethylation in ulcerative colitis-related colorectal cancer. *Carcinogenesis* 33(10):1889–1896.
35. Zhang Q, et al. (2011) TGF-β regulates DNA methyltransferase expression in prostate cancer, correlates with aggressive capabilities, and predicts disease recurrence. *PLoS One* 6(9):e25168.
36. Miller CH, Maher SG, Young HA (2009) Clinical use of interferon-gamma. *Ann N Y Acad Sci* 1182:69–79.
37. Zaidi MR, Merlino G (2011) The two faces of interferon-γ in cancer. *Clin Cancer Res* 17(19):6118–6124.
38. Vlková V, et al. (2014) Epigenetic regulations in the IFNγ signalling pathway: IFNγ-mediated MHC class I upregulation on tumour cells is associated with DNA demethylation of antigen-presenting machinery genes. *Oncotarget* 5(16):6923–6935.
39. Milner E, Barnea E, Beer I, Admon A (2006) The turnover kinetics of major histocompatibility complex peptides of human cancer cells. *Mol Cell Proteomics* 5(2):357–365.
40. Pastor MD, et al. (2013) Identification of proteomic signatures associated with lung cancer and COPD. *J Proteomics* 89:227–237.
41. Luo W, Semenza GL (2011) Pyruvate kinase M2 regulates glucose metabolism by functioning as a coactivator for hypoxia-inducible factor 1 in cancer cells. *Oncotarget* 2(7):551–556.
42. Chao A, et al. (2013) Tumor stress-induced phosphoprotein1 (STIP1) as a prognostic biomarker in ovarian cancer. *PLoS One* 8(2):e57084.
43. Wang TH, et al. (2010) Stress-induced phosphoprotein 1 as a secreted biomarker for human ovarian cancer promotes cancer cell proliferation. *Mol Cell Proteomics* 9(9):1873–1884.
44. Anania MC, et al. (2013) S100A11 overexpression contributes to the malignant phenotype of papillary thyroid carcinoma. *J Clin Endocrinol Metab* 98(10):E1591–E1600.
45. Hao J, et al. (2012) Selective expression of S100A11 in lung cancer and its role in regulating proliferation of adenocarcinomas cells. *Mol Cell Biochem* 359(1-2):323–332.
46. Yu W, et al. (2015) Clonal deletion prunes but does not eliminate self-specific αβ CD8(+) T lymphocytes. *Immunity* 42(5):929–941.
47. Schliekelman MJ, et al. (2015) Molecular portraits of epithelial, mesenchymal, and hybrid States in lung adenocarcinoma and their relevance to survival. *Cancer Res* 75(9):1789–1800.
48. Sun M, et al. (2009) HER family receptor abnormalities in lung cancer brain metastases and corresponding primary tumors. *Clin Cancer Res* 15(15):4829–4837.
49. Taguchi A, et al. (2011) Lung cancer signatures in plasma based on proteome profiling of mouse tumor models. *Cancer Cell* 20(3):289–299.
50. de Verteuil D, et al. (2010) Deletion of immunoproteasome subunits imprints on the transcriptome and has a broad impact on peptides presented by major histocompatibility complex I molecules. *Mol Cell Proteomics* 9(9):2034–2047.